Received: 2 June 2017 | Accepted: 11 September 2017

DOI: 10.1111/jace.15237

ORIGINAL ARTICLE

Journal of the American Ceramic Society

Simulations of the surfaces of soda lime aluminoborosilicate glasses exposed to water

Stephen H. Garofalini | **Ming Tai Ha** | **Joelyn Urraca**

Department of Materials Science and Engineering, Rutgers University, Piscataway, New Jersey

Correspondence
Stephen H. Garofalini, Department of Materials Science and Engineering, Rutgers University, Piscataway, NJ.
Email: shg@glass.rutgers.edu

Funding information
Nuclear Energy University Programs, Grant/Award Number: DE-NE0008597

Abstract

Molecular dynamics simulations of 7 compositionally different sodium calcium alumino-borosilicate glasses showed formation of ^{4}B and ^{5}Al more consistent with experimental data without compromising the other structural features that match experimental results observed in recent simulations of these glasses. Analysis of the dry surfaces of these glasses show a lack of ^{4}B in the top 5-6 Å of the surface in comparison to the bulk concentration for all glasses and no ^{5}Al. Upon exposure to water, the simulations show that the ^{3}B in the top 5-6 Å of the glasses are preferentially attacked, decreasing the number of B bonds to O originally from the glass, indicating a change in the glass network. Inclusion of all B–O bonds in the top 5-6 Å (i.e., including O from water) shows a decrease in ^{3}B but an increase in ^{4}B that is consistent with NEXAFS analysis, which the simulations show are hydroxylated. There is an increase in the concentration of ^{3}Al in the dry surface in comparison to the bulk, but exposure to water converts almost all of these ^{3}Al to ^{4}Al. Hydroxyl concentrations vary from 2.6/nm^2 to 4.1/nm^2, with SiOH and BOH dominating these surface hydroxyls. Upon exposure to water, network linkages to B are preferentially ruptured. This, and the preferential loss of the nonbridging oxygen sites attached to Na, provide atomistic evidence of the initial stages of removal of B and Na from glass surfaces exposed to water.

KEYWORDS
glass, simulation, structure, surface

1 | INTRODUCTION

Soda-lime alumino-borosilicate glasses have found applications in many fields[1-4] and there is renewed interest in the structure and properties of these glasses.[5-14]

In a recent paper,[15] the bulk structure of aluminoborosilicate glasses containing 10%-20% Ca and Na modifiers was explored using molecular dynamics simulations of systems containing ~20 000 atoms. Over a dozen compositions and densities were studied. The compositions were not designed to match any particular experiment, since there are many with varied compositions. However, the trends and general conclusions observed in those different experimental studies were considered. A brief summary of the recent paper[15] indicates a number of simulation results that were consistent with experimental data of the structure of bulk glasses: the bond lengths of each cation to oxygen was consistent with experiment; an increase in the Al_2O_3/B_2O_3 results in a decrease in the BO_4 (often called N4 or ^{4}B) concentration at constant modifier content, consistent with Wu and Stebbins[14]; an increase in the Ca concentration caused an increase in the ^{5}Al and a decrease in the ^{4}B, similar to experiment[11,14]; an increase in the Na concentration increased the ^{4}B, similar to experiment[12,14]; using the local coordination number, Na preferentially associates with Al > Si > B, similar to experiment[16]; higher charge Ca enables a reduction in Al or B avoidance, similar to experiment[17,18]; a decrease in the glass density leads to a

decrease in the ^{5}Al, similar to experiments on fictive temperature on ^{5}Al concentration.[13] Based on coordination numbers, Ca also was seen to prefer to aggregate first around Al, then B, then Si. The simulations showed that Ca tends to promote the formation of BO_3 (or ^{3}B) and Na tends to promote the formation of ^{4}B. The similarities between simulation and experiment enabled further evaluation of the network former to network modifier coordinations and distances.

However, while the general trends in the previous work were consistent with experimental data, the concentrations of the ^{5}Al and ^{4}B were higher than that observed experimentally. Given that the potentials use in the simulations involve multibody terms (2-body and 3-body), it appeared that the 3-body forms used in the previous paper might be too soft and led to the high concentrations of ^{5}Al and ^{4}B. In order to correct this result, we performed additional simulations of the same glasses presented in the previous paper with modified 3-body terms centered on the Al and the B in order to obtain coordination numbers more in line with NMR data and determine the effect of this change on the other behavior previously reported. Results show that the modified 3-body terms corrected the high concentration of ^{5}Al and ^{4}B without sacrificing similarity to the other properties previously shown to be consistent with experiment. For the sake of brevity, we will refer to the samples generated with new 3-body terms centered on the Al and the B as the "new" samples, and refer to the samples generated with previous parameters studied in the previous paper as the "old" samples.

In addition to structural analyses of the bulk samples, glass/vacuum interfaces were made and the structures in the surfaces of the glasses were also evaluated. These surfaces were then exposed to water and the effect of the reactions between the water and the glass surfaces were analyzed with respect to the changes in the surface structure.

2 | COMPUTATIONAL PROCEDURE

The multibody potential previously used in reference[15] in the study of these multicomponent glasses was used in the current molecular dynamics (MD) simulations, with all parameters and glass compositions and sizes and quenches being the same except for the 3-body terms centered on the Al for the O–Al–O interactions and B in the O–B–O interactions. Except for these latter aspects regarding the modification of the 3-body term centered on Al and B, this potential and parameters have been used in simulations of multicomponent silicates such as sodium silicates,[19,20] sodium aluminosilicates,[21,22] calcium aluminosilicates,[23-25] and sodium calcium alumino-borosilicate glasses,[26] mostly with interest in the surface and interfacial properties.

The 2-body and 3-body interactions are calculated using the following form for the 2-body term,

$$V_{ij}^{\mathrm{BMH}} = A_{ij}\exp\left(\frac{-r_{ij}}{\rho_{ij}}\right) + \left(\frac{z_i z_j e^2}{r_{ij}}\right)\mathrm{erfc}\left(\frac{r_{ij}}{\beta_{ij}}\right) \quad (1)$$

and the 3-body term centered on O, Si, Al, or B is given by:

$$V_{jik}^{3-\mathrm{body}} = \lambda_{ij}^{1/2}\lambda_{ik}^{1/2} * \exp\left[\frac{\gamma_{ij}}{(r_{ij}-R_{ij})} + \frac{\gamma_{ik}}{(r_{ik}-R_{ik})}\right]\Theta_{jik}, \quad \text{if } r_{ij} < R_{ij} \text{ and } r_{ik} < R_{ik}, \quad (2)$$

else,

$$V_{jik}^{3-\mathrm{body}} = 0 \quad (3)$$

The angular component Θ_{jik} centered on the O, Si, or B is given by,

$$\Theta_{jik} = \left(\cos\theta_{jik} - \cos\theta_{jik}^0\right)^2 \quad (4)$$

where θ_{jik} is the angle formed by the ions j, i, and k, with the ion i as the vertex. θ_{jik}^0 is 109° centered on O or Si and 120° centered on B. The angular component for O–Al–O is given by,

$$\Theta_{jik} = \left(\left(\cos\theta_{jik} - \cos\theta_{jik}^0\right)\sin\theta_{jik}\cos\theta_{jik}\right)^2 \quad (5)$$

and θ_{jik}^0 is 109°. Each glass composition went through a melt/quench procedure similar to that of the previous paper,[15] with periodic boundary conditions is three dimensions and a timestep of 1 fs. The system sizes were ~65 Å × ~65 Å × ~65 Å with ~20 000 atoms each. The compositions and labeling protocol for the rest of the paper are given in Table 1. While the quench rate used here (and previously[15]) is fast (~10^{13} K/s), we also redid some of the previous compositions with a quench rate of ~10^{11} K/s

TABLE 1 Composition of the glass samples

Name	SiO_2 (mol%)	Al_2O_3 (mol%)	B_2O_3 (mol%)	CaO (mol%)	Na_2O (mol%)	Total number of atoms
Al5-B15	60	5	15	10	10	19 998
Al10-B10	60	10	10	10	10	19 998
Al15-B5	60	15	5	10	10	19 998
Ca20	60	10	10	20	0	20 000
Ca10	70	10	10	10	0	19 998
Na20	60	10	10	0	20	19 998
Na10	70	10	10	0	10	19 998

with no significant change in results. This lack of difference in these quench rates was also observed by Adelstein and Lordi[27] in their simulations of multicomponent glasses. However, the previous study also used different densities for additional compositions to mimic glasses with different glass transition temperatures and found results consistent with experiment.[15]

The 3-body term centered on Al used in the previous paper[15] had parameters for λ_{ij}, γ_{ij}, and R_{ij} equal to 0.024 fJ, 2.8 Å, and 3.0 Å, respectively. The new values of λ_{ij}, γ_{ij}, and R_{ij} are 0.035 fJ, 1.8 Å and 3.2 Å, respectively. For the case of B, the old values for λ_{ij}, γ_{ij}, and R_{ij} were 0.024 fJ, 2.8 Å, and 3.0 Å, while the new values for λ_{ij}, γ_{ij}, and R_{ij} are 0.035 fJ, 1.8 Å and 2.5 Å, respectively. Prior to performing the simulations of the glasses with the new 3-body parameters on the Al, both α-Al_2O_3 and γ-Al_2O_3 were simulated in NPT (constant number, pressure, temperature) simulations and shown to be stable, similar to earlier work with the previous 3-body parameters. The Al–O bond length in α-Al_2O_3 is 1.90 Å in the simulations, similar to the ab-initio data of 1.92 Å,[28] whereas the Al–O bond lengths in γ-Al_2O_3 are 1.81 Å and 1.92 Å in the simulations, similar to the ab-initio data of 1.81 Å and 1.94 Å.[28]

The average densities and Poisson's ratios and Young's modulus of each are given in the supplementary file, Table S1. Direct comparison to experiment is not available, but the Poisson's ratios appear to be within the expected range of silicate glasses (−0.22 to −0.23) while the Young's modulus appears somewhat high for silicate glasses, which is consistent with the higher Young's modulus observed for SiO_2 glass using this potential.

After making the glasses with the new 3-body terms on the Al and B ions, analyses similar to the earlier work was done. The pair distribution function (PDF) was calculated for individual cation-oxygen pairs (Si/Al/B/Na/Ca–O) and network former-network modifier pairs (Al/B/Si–Ca/Na) (for the sake of brevity in not having to separately add the word "intermediate" in discussions that include Al, we are including Al as a network former in these glasses). The coordination numbers for cation-oxygen pairs and network former to network modifiers were calculated out to the distance of the first minimum following the first peak (maximum) in the PDF.

The surfaces were made in the familiar manner similar to previous simulations of glass surfaces,[29-33] although the glasses were first relaxed at 298 K under 1 atm constant pressure simulations. Briefly, the periodic boundary condition in the z dimension was removed concurrent with freezing the bottom 12 500 atoms, allowing all others to relax to the conditions afforded by creation of the surface in the $+z$ direction. Our previous simulations of glass surfaces showed that surface relaxation extended only ~15 Å below the free surface[30,31]; the depth of the mobile (non-frozen) atoms is ~27 Å). The frozen atoms do not respond to the forces from other atoms but do respond to changes in dimension during cooling. Each resultant glass was heated to 1000 K for 50 000 timesteps followed by cooling to 500 K then 300 K, each also at 50 000 timesteps. The structure of the surface was analyzed by evaluation of the pair distribution functions of the ions and coordination numbers and concentrations of the ions in three separate regions: top 5-6 Å of the surface, labeled "surf"; ions in the next 10 Å (5 Å-15 Å below the outer surface), labeled "sub"; and ions in the region 25 Å–35 Å below the outer surface, labeled "bulk." The types of bridging and nonbridging oxygens were determined in the surface region as well as the ring structures of the network forming Si, Al, and B ions.

In addition, these glasses were exposed to water in order to evaluate changes in the surface species before and after such exposure. An approximately 2 nm layer of water was placed above the surface of each glass followed by a simulation run of 1×10^7 time steps at 298 K. Analysis involved evaluation of the change in the coordination of the B and Al species in the surface (top 5-6 Å) and the types of bridging and nonbridging oxygens similar to the dry surface analysis, as well as the formation of hydroxyls in each surface and the change in the ring structures prior to and post exposure to water.

3 | RESULTS AND DISCUSSION

The cation-oxygen and former-modifier interatomic distances calculated using the new 3-body term on Al and B are equal to those of the previous publication (within 0.001 Å of the previous data) and agree well with experimental and simulation results mentioned in the previous paper.[17,34-37] The Si–O first peak is at 1.61 Å; the B–O first peaks are at 1.365 Å for ^{3}B and 1.45 Å for ^{4}B; the Al–O peak is at 1.70-1.71 Å. Figure 1 shows the PDF for B–O first neighbor peak, showing the formation of the ^{4}B with composition as the higher distance shoulder. The shape of this curve is different from that observed in the previous paper[15] caused by the more reasonable concentration of these ^{4}B in the current simulations, as shown in Table 2.

The most noticeable change in the current simulations with the new 3-body terms is in the concentration of 4-, 5-, and 6-coordinated Al (^{4}Al, ^{5}Al, and ^{6}Al, respectively) and 3- and 4-coordinated B. Table 2 shows the new data regarding B, Al and Si coordination numbers to oxygen and Figure 2 shows a histogram of the concentration of ^{4}B, ^{5}Al, and non-bridging oxygens (NBO) in the seven glasses. In comparison to the previously published data, the ^{4}B concentrations decrease between 30%-60% and the decrease in the ^{5}Al is even more significant; both sets of results are

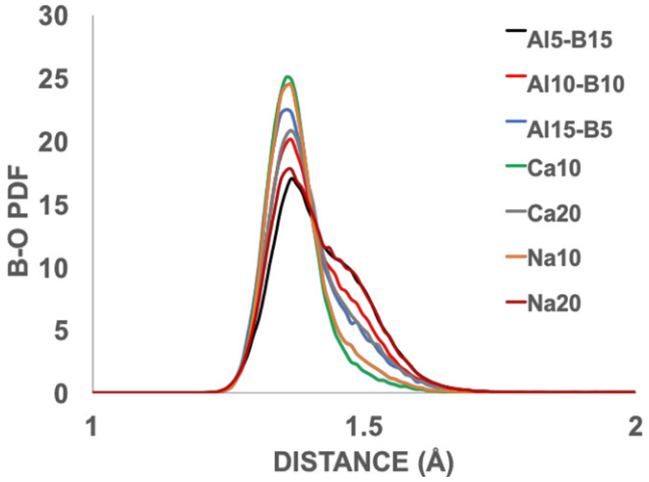

FIGURE 1 First peak of the B–O pair distribution function (PDF) for the glasses showing the shorter distance peak consistent with B_3 versus the longer distance for the N4 Boron and the changes with composition [Color figure can be viewed at wileyonlinelibrary.com]

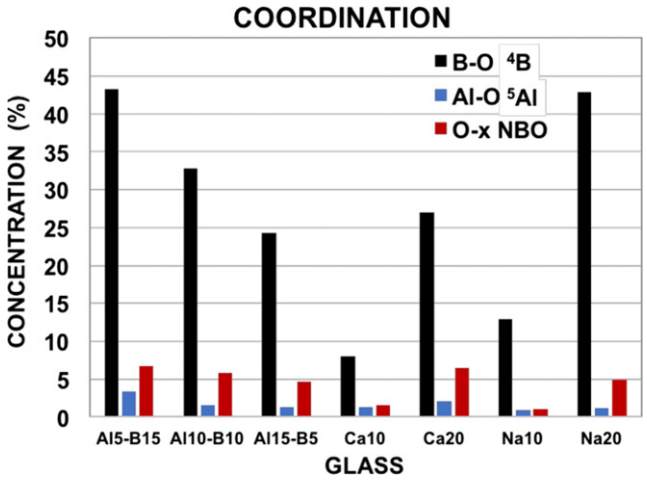

FIGURE 2 Concentration of ^{4}B, ^{5}Al, and nonbridging oxygens (NBO) as a function of glass composition. The figure shows the effect of increasing the Al_2O_3 concentration (from Al5-B15 to Al15-B5) on decreasing the ^{4}B concentration, the greater effect of Na on formation of ^{4}B than Ca addition (Ca10 (20) vs. Na10 (20)) and the higher concentration of NBO in the Ca glasses (Ca10, Ca20) vs. the Na glasses (Na10, Na20), all consistent with experiment. Compositions labels are given in Table 1 [Color figure can be viewed at wileyonlinelibrary.com]

TABLE 2 Concentration (%) of B–O, Al–O, and Si–O coordination numbers for the glasses

B–O	Coord #3	Coord # 4
Al5-B15	56.7	43.3
Al10-B10	67.2	32.8
Al15-B5	75.7	24.3
Ca10	92	8
Ca20	73	27
Na10	87.1	12.9
Na20	57.1	42.9

Al–O	Coord # 3	Coord # 4	Coord # 5
Al5-B15	0.3	96.4	3.3
Al10-B10	0.2	98.3	1.6
Al15-B5	0.4	98.3	1.3
Ca10	2.1	96.5	1.3
Ca20	0.2	97.7	2.1
Na10	0.8	98.3	0.9
Na20	0.2	98.6	1.2

Si–O	Coord # 4	Coord # 5
Al5-B15	98.8	1.2
Al10-B10	99.3	0.7
Al15-B5	99.6	0.4
Ca10	99.8	0.2
Ca20	99.3	0.7
Na10	99.6	0.4
Na20	98.8	1.2

All other coordinations equal 0.

much more consistent with the experimental data.[11,14,18] The overall trends also still match the changes in ^{4}B and ^{5}Al as a function of composition seen experimentally and in the previous simulations. The concentration of ^{6}Al went from ~0.24%-0.94% in the previous glasses to 0.0% in the glasses presented here. The NBO also show results consistent with experiment[14]: with increasing Ca concentration there is an increase in the NBO concentration (Ca10 to Ca20, and Na20 to Ca20). In this new work, the other trends remain the same as the previous work, consistent with experiment, and the concentration ^{4}B and ^{5}Al species are much more consistent with experiment. These results indicate the importance of the values of the 3-body terms on the resultant structure.

From Table 2 and Figure 1, the PDF of the B–O bond of the compositions Al5-B15, Al10-B10, and Al15-B5 of the new samples, with increasing ratio of Al_2O_3/B_2O_3, the ratio of BO_3/BO_4 increases caused by a decrease in the ^{4}B concentration, consistent with the previous paper[15] and experimental data[38] for Na_2O–Al_2O_3–B_2O_3 glasses. Wu and Stebbins similarly showed that at equal concentrations of CaO and Na_2O, increasing Al_2O_3/B_2O_3 ratio lowers the BO_4 content.[14] In addition, with the new 3-body term on Al and fewer ^{5}Al, this trend of fewer BO_4 with increasing Al at constant Na and Ca is enhanced in comparison to the previous paper.

Table 2 and Figure 2 also show the effect of CaO-only additions and Na_2O-only additions on the concentration of BO_4, with Na_2O having a greater effect on enhancing BO_4

formation. This is consistent with the experiments by Wu and Stebbins who also show that Na has a greater effect on the formation of BO_4 than does Ca.[14] Similar to their data on the concentration of NBOs as a function of Ca versus Na in their Table 2, our Figure 2 shows an increase in NBO with increasing Ca and more NBO in the Ca glasses than the Na glasses (Ca10 and Ca20 vs. Na10 and Na20).

The previous work[15] showed that the mean coordination of the network former cations to Ca was Al > B > Si and the mean coordination of the network former cations to Na was Al > Si > B, the latter being similar to experimental data.[16] The current data gives the same result, as shown in Figure 3, indicating the order of preference for the modifiers to the network forming cations. Figure 3 has the average coordination to the Na ions divided by 2 in the figure, so the actual coordination numbers to Na are twice as high, as expected for having twice as many Na ions as Ca ions in the glass for equal mole concentrations of these two oxides. With increasing Al_2O_3/B_2O_3 ratio in Al5-B15 < Al10-B10 < Al15-B5, there is a decrease in the average coordination number of all 3 network formers to Ca or Na (note that the differences in the peak heights for Na in Figure 3 would be doubled if plotted in actual numbers). This decrease is also indicated in Figure 4 which shows the concentration of the network formers that have no Ca or Na within the first peak in the PDFs. Al has fewer ions with no Ca neighbors, followed by B, then Si, indicating the preference of Ca for Al > B > Si; in the Na case, the order for Na preference is Al > Si > B. In addition, it is seen that with increasing the Al_2O_3/B_2O_3 ratio in the glasses, there is an increase in the concentration of B with no

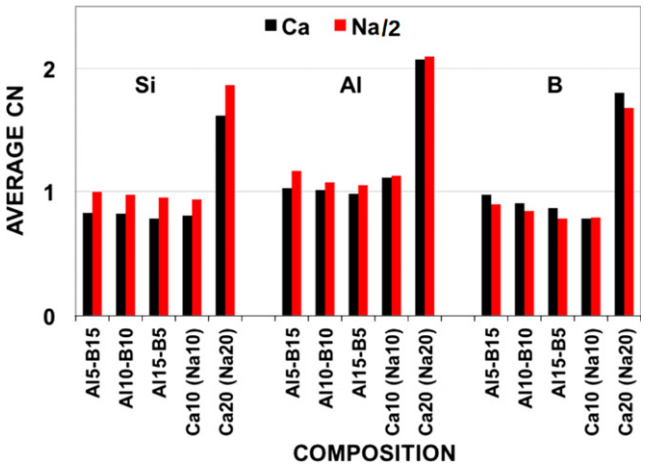

FIGURE 3 Average number (coordination number (CN)) of network modifiers Ca and Na around each network former (Si, Al, B) as a function of composition. The actual Na values are divided by 2 in the graph for clarity. The order of preferential attraction of Na is to Al > Si > B; for Ca, the order is Al > B > Si [Color figure can be viewed at wileyonlinelibrary.com]

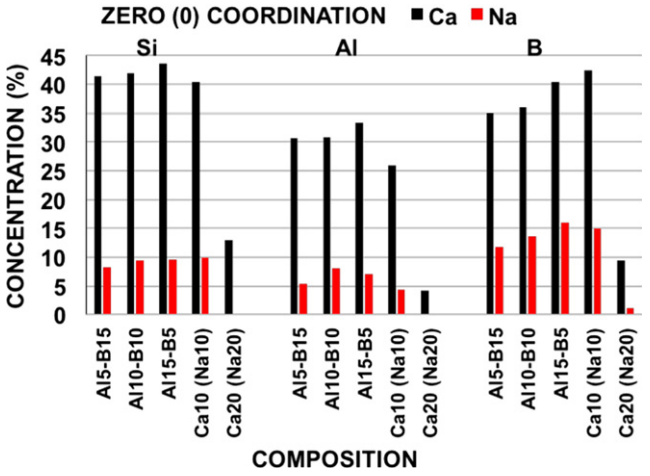

FIGURE 4 Concentration of each network former, Si, Al, and B, that has no Na ions (red) or no Ca ions (black) within the first peak of the former-modifier pair distribution function. There are far more network species with no Ca ions than with no Na ions (even taking into account twice as many Na ions than Ca in the glasses for the same molar concentration), indicating the preference for the network species to associate with Na rather than Ca. The Al have the smallest number with no Ca or no Na nearby, indicating that Ca and Na have a higher preference to go to Al than to the other two network formers. For Na20 all Si and Al have a Na neighbor [Color figure can be viewed at wileyonlinelibrary.com]

modifier within the first B-modifier peak in the pair distribution function.

Increasing the Al_2O_3/B_2O_3 ratio causes two potentially related results: there is a decrease in the average coordination number of B to both the Na and Ca modifiers and there is a decrease in the concentration of ^4B, as shown in Table 2. Interestingly, the reduced (by 2 in the figure) B-Na coordinations are lower than the B–Ca coordination, whereas those reduced values for Na are greater than Ca coordinated to Si and Al (Figure 3) (while there are always more Na around the network formers than Ca, this subtle difference in preference would have been less obvious had the Na values not been reduced by a factor of 2 for the graph).

With glasses Al5-B15, Al10-B10, and Al15-B5, where the charges on the +3 cations are equally compensated by the 10% CaO plus 10% Na_2O, or by the Ca20 or the Na20 glasses, a 5%-7% concentration of NBO exist; the NBO concentration decreases with increasing Al due to the preference of each modifier to go to the Al ions prior to the B or Si. In the Ca10 (zero Na) and Na10 (zero Ca) glasses, with a deficiency of modifiers to compensate the +3 network formers, the NBO concentration is low (~1%-1.5%). In those cases, however, the concentration of oxygen triclusters increases to slightly over 3%. Tricluster oxygen have been proposed in cases where modifier content is insufficient to compensate the +3 cations,[39,40] although

concentrations of triclusters below 2% are difficult to observe in NMR[40]. Tricluster oxygen is seen with increasing Al_2O_3 or with increasing Ca in the simulations, similar to experiment.[39]

The effect of changing the three-body parameters on Al and B has produced results more consistent with the concentrations of ^{5}Al and ^{4}B observed experimentally, but did not change the main conclusions drawn in the previous paper that matched the effect of compositional changes on the structures of these glasses.

3.1 | Surface structure

Evaluation of the surfaces of these glasses showed significant changes in the concentration of ^{4}B and ^{5}Al in the surface in comparison to the bulk. There were no ^{5}Al in the "surface" region of the glasses as labeled in the Computational Procedure section, although they are present in the subsurface and bulk. There are 3 coordinated Al in the surface.

Figure 5A-C shows the first peak in the B–O PDFs of several of the glasses. The curves have been normalized to obtain the same peak maximum for the figures. The high distance shoulder in the figures is indicative of the ^{4}B–O distance. Figure 6 shows the concentration of ^{4}B in the surface, subsurface, and bulk regions of all of the glasses, corroborating the significant decrease in the ^{4}B in the surface implied by the PDFs in Figure 5. Clearly the number of ^{4}B decreases significantly from the bulk to the surface for all of the glasses except the Ca10 and Na10 glasses. Ca10 and Na10 glasses have excess $^+$3 cations that are not charge compensated by the modifier contents and have the fewest ^{4}B in any location in the glass. The largest loss of ^{4}B occur in those glasses with the largest B concentration.

Figure 7 shows that there is a slight increase in the concentration of B in the surface and subsurface in most of the glasses. Al slightly increases at the surface for some glasses and slightly decreases for others. Na and Ca do not show any particular preference for the glass surface, providing evidence of the importance of the specific locations of the Na ions with respect to B in the formation of ^{4}B. The lower concentration of Na in the surface is surprising given the prevalence of Na at the surface of sodium silicate binaries.[41,42]

Consideration of the type of bridging oxygen associated with the +3 cations in the surface is shown in Figure 8A. Because of the higher concentration of Si in the surface, Si–O bonds to Al or B dominate; of the +3 to +3 cations, the AlOB bonding dominates these other surface species. Figure 8B shows the change in the surface concentration of these species post water exposure and will be discussed below.

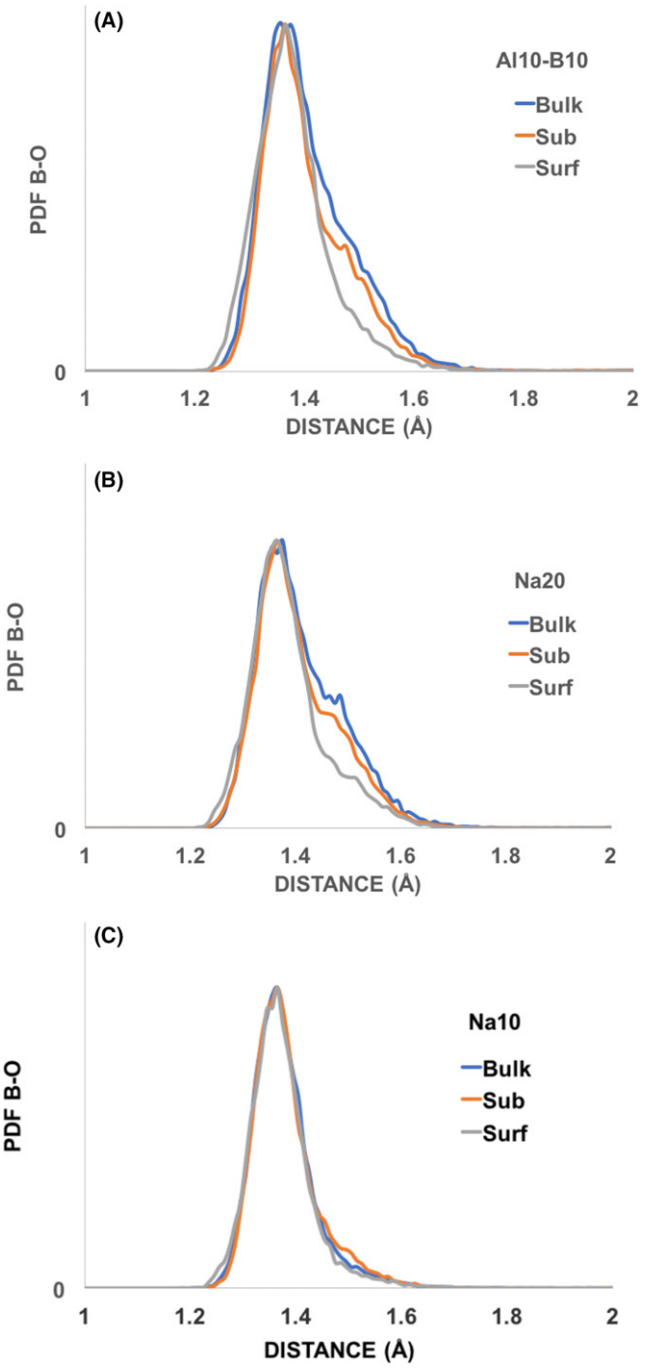

FIGURE 5 B–O PDFs of the first peak for B located in the bulk, subsurface, and surface of several glass compositions shown on each Figure 5A-C. Peak maxima are normalized to that of the bulk value enabling easier comparisons of the long distance shoulder that is indicative of ^{4}B [Color figure can be viewed at wileyonlinelibrary.com]

3.2 | Exposure to water

Figure 9A shows the change per unit volume in the original ^{3}B and ^{4}B concentrations in the glass surfaces (top 5-6 Å) for B attached only to O from the glass prior to exposure to water and post exposure to water; that is, B–O bonds to O from water (Ow) are not included in 9(A) in

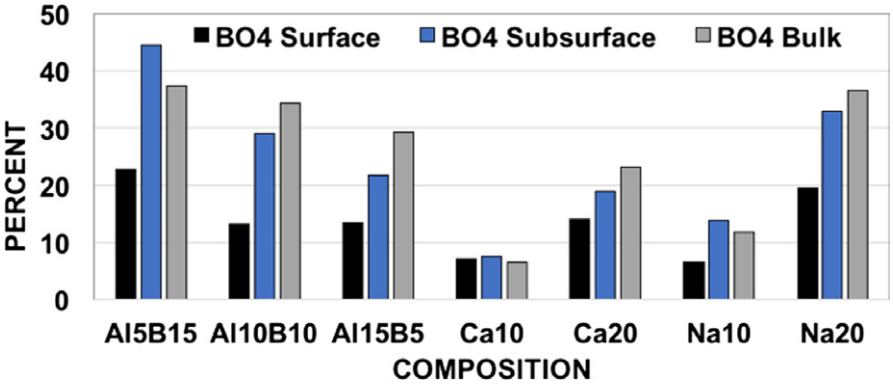

FIGURE 6 Concentration of ^{4}B in the surface, subsurface, and bulk of the glasses, showing the decrease in the ^{4}B in the surface with respect to the bulk, similar to the implications of the PDFs in Figure 5 [Color figure can be viewed at wileyonlinelibrary.com]

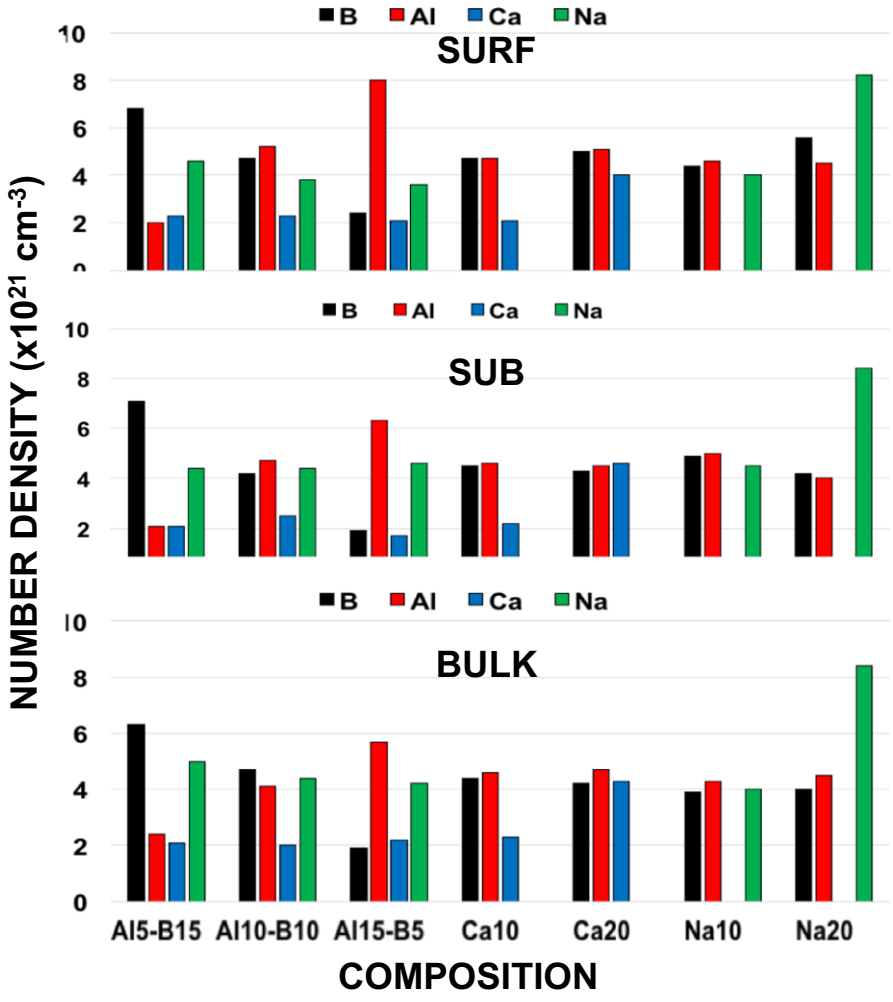

FIGURE 7 The number density of B (black), Al (red), Ca (blue), and Na (green) for the surface, subsurface, and bulk regions of each of the glasses. There is a very slight increase in the B concentrations in the surface and subsurface in comparison to the bulk for several glasses and almost no change in the concentrations of Na and Ca [Color figure can be viewed at wileyonlinelibrary.com]

order to show the change in the network bonding between B and O. Figure 9A shows the loss of B–O bonds for those B attached to glass oxygen. These B changed to 1 and 2 coordinated B. There is not any significant decrease or increase in the ^{4}B's using this criterion, indicating that the ^{3}B's are the borons that are preferentially attacked in the outer surfaces. Figure 9B shows the change in the original ^{3}B and ^{4}B concentrations in the glass surfaces attached to any O from the glass or water prior to and post water exposure. Inclusion of bonding to O from the water (Ow) still shows a decrease in the ^{3}B species in the glass surface, but also shows that inclusion of the Ow attached to B causes an increase in the concentration of ^{4}B in the outer surface.

This increase at the concentration of ^{4}B in the outer glass surface is consistent with the NEXAFS data discussed by Schaut et al[43] showing increased ^{4}B content in their glass surfaces.

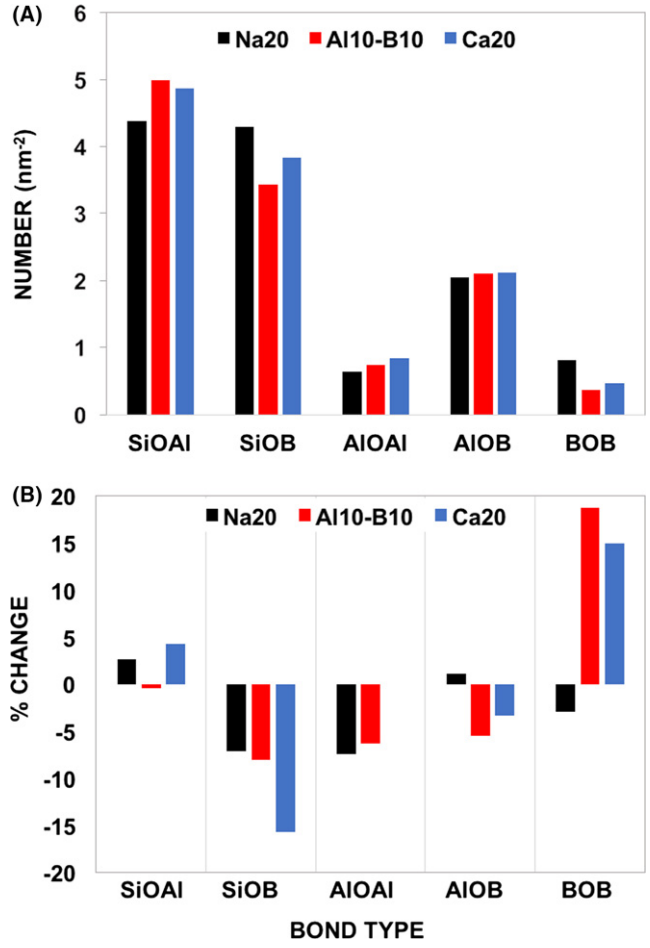

FIGURE 8 (A) Number density of bridging oxygen at the dry surface connected to a +3 cation in the three glasses that have equal concentrations of Al and B and full charge compensation by the modifier ions. Of course, Si to Al or B dominate, whereas AlOB triples dominate the direct +3 cation linkages. (B) Percent change in the concentration of bridging bonds in the same 3 glasses as in (A) after exposure to water [Color figure can be viewed at wileyonlinelibrary.com]

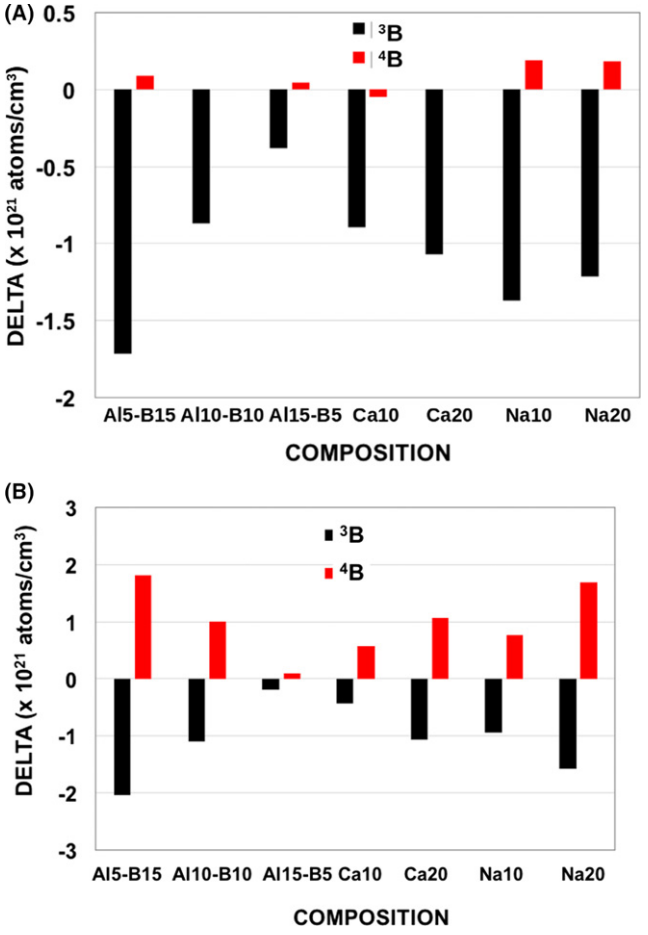

FIGURE 9 (A) Delta (change) per unit volume in the original ^{3}B and ^{4}B concentrations in the glass surfaces (top 5-6 Å) attached only to O from the glass prior to exposure to water and post exposure to water, showing loss of B–O bonds for those B attached to glass oxygen. These B changed to 1 and 2 coordinated B. Generally, the ^{3}B's are the borons that are preferentially attacked in the outer surfaces. (B) Percent change (delta) in the original ^{3}B and ^{4}B concentrations in the glass surfaces attached to any O from the glass or water prior to water exposure and post water exposure. Inclusion of bonding to O from the water causes an increase in the concentration of ^{4}B in the outer surface [Color figure can be viewed at wileyonlinelibrary.com]

An example of the reactions occurring at the surface is shown in Figure 10A-D. Figure 10A shows the colors of the atoms (blue Si, red Al, green B, cyan Owater (Ow), grey O from the glass, and white protons; Na and Ca are removed from the image); the circle containing two ^{3}B and an H_2O. In 10(B) this H_2O reacts with the BOB bond forming 2 BOH's (with the original O from the bond on the lower B and the Ow (and H) forming the OH on the upper B). In 10(C) another H_2O reacts with the upper B, forming a ^{4}B. In 10(D), another H_2O reacts with the AlOB of the lower B, forming an AlOH and a BOH as this B becomes a ^{4}B. Hence, two ^{4}B's form from these two original ^{3}B's. The images also show the relative ease with which the water molecule attaches to a ^{3}B to form a ^{4}B. This is due to the open structure of the ^{3}B that enables the 4th O to attach even though there is a trigonal 3-body term centered on the B.

In addition, the connection of the two B's caused by the O from the water molecule is an example of a cause for the increase in BOB triples shown in Figure 8B for some glasses. Figure 8B shows the percent change in these bridging bonds prior to and post exposure to water for the 3 glasses that have equal concentrations of Al and B and full charge compensation by the modifier ions. There is a significant decrease in the SiOB and AlOB bonding given their higher concentrations in the dry glasses in comparison to AlOAl. The change in SiOSi bonds (not shown) is ~1.2% and much smaller than these other bridging bond types. Such results indicate a weakness in those bridging bonds containing a B. The increase in the BOB bonds for

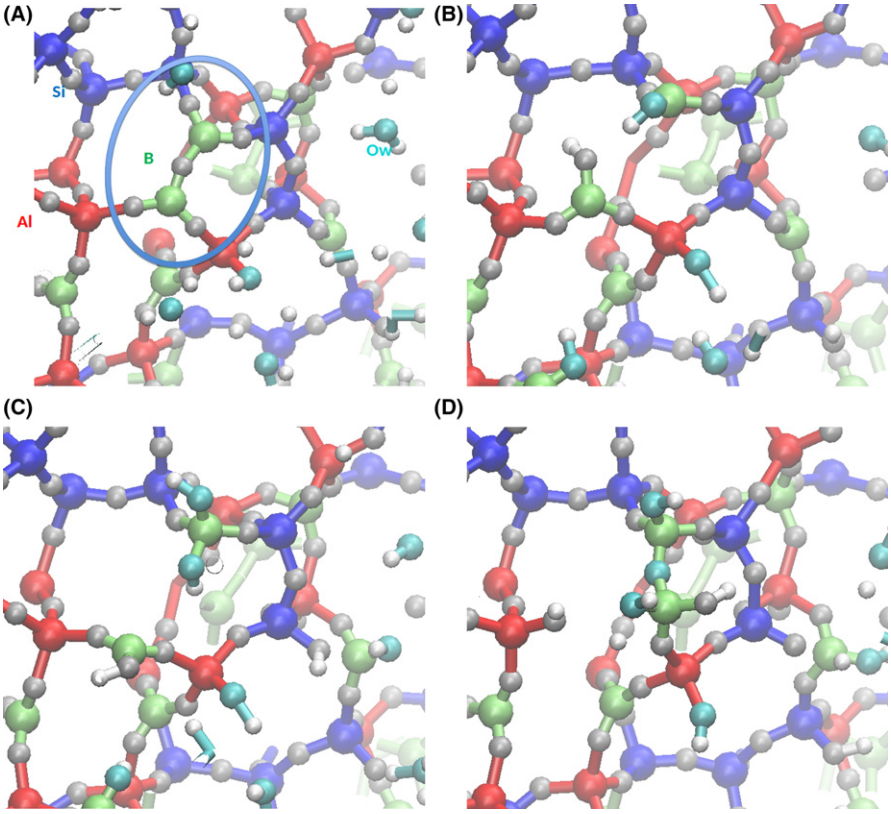

FIGURE 10 Reactions of B in the surface with water to change the 2 ^{3}B in (A) to ^{4}B's by the end of the reaction in (D). Si = blue, Al = red, B = green, O in glass = gray, O in water = cyan. See text for detailed explanation [Color figure can be viewed at wileyonlinelibrary.com]

the two glasses may be related to the formation of ^{4}B that connect via the water oxygen (similar to that in Figure 10D, but those B's started in a BOB triple). However, considering the 2 B's in the bottom left of Figure 10D, one could imagine a water molecule breaking the lower AlOB bond in the left-most location, enabling the B to shift to the B on its right, forming a BOB bond.

The Al do not show ^{5}Al in the surface, but do show the formation of ^{3}Al. Upon exposure to water, the change in ^{3}Al into ^{4}Al is almost complete for all of the compositions, as shown in Figure 11.

The concentration of hydroxyls is shown in Figure 12, with a range from 2.6-4.1 nm^{-1}, with the lowest number in the high Al glass and the highest numbers in the high B and high Na glasses. The hydroxyls that form are preferentially on Si and B, with fewer on the Al, as shown in Figure 13. At constant concentrations of Al and B (at 10% each in the Al10-B10, Ca10, Ca20, Na10, and Na20 glasses) the concentration of SiOH is fairly constant; however, as expected, increased Al/B ratio shows increased AlOH and decreasing BOH. In addition, the concentration of AlOH in the surface is smaller for the Ca-only glasses versus the Na-only glasses.

In addition to hydroxyls, the surface region of the glasses contains non-bridging oxygen (NBO) that are coordinated with one network former and a network modifier (or proton in the case of the wet surfaces), as well as O attached to only a network former with no modifier within

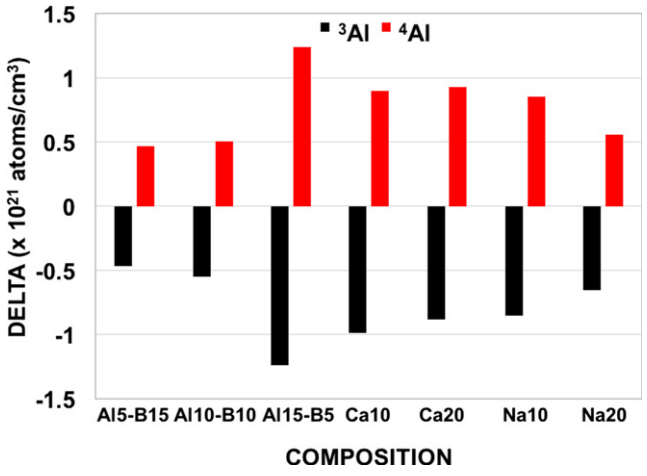

FIGURE 11 Change (delta per unit volume) in the concentration of ^{3}Al and ^{4}Al in the surface prior to water exposure and post water exposure (this includes the O from water), showing the nearly complete change from ^{3}Al to ^{4}Al [Color figure can be viewed at wileyonlinelibrary.com]

the former-modifier neighbor cut-off distance (that we will call singly-coordinated oxygen, or SCO). Figure 14 shows the sum of these different NBO species for the network formers for the dry surfaces versus the wet surfaces. The sum of all NBO species for all of the glass surfaces increases for each network former in going from the dry to the wet surfaces, with the Si-NBO dominating all compositions. In those glasses with equivalent Al and B

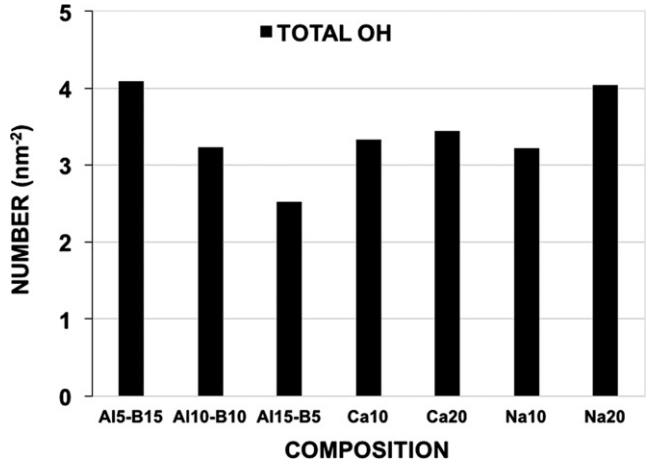

FIGURE 12 Hydroxyl concentrations in the glasses

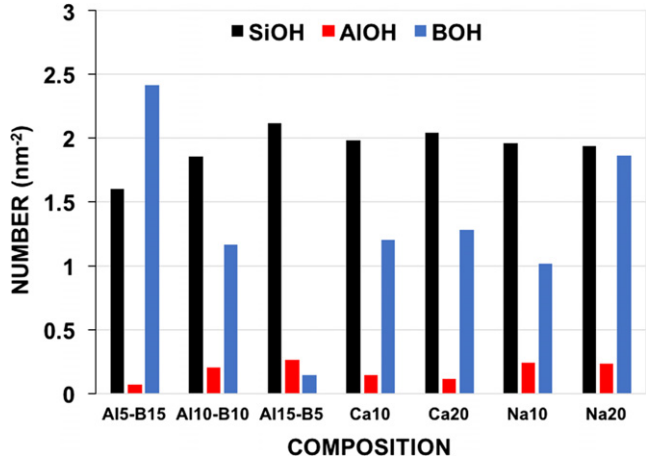

FIGURE 13 Number density of SiOH, AlOH, and BOH in the glass surfaces [Color figure can be viewed at wileyonlinelibrary.com]

concentrations, B to NBO dominate after Si-NBO. This may seem contradictory given the earlier discussion showing the preference for the Na and Ca to Al prior to B, but that preference includes bridging oxygen (AlOAl, etc.) that are in much higher concentration than the Al-NBO or B-NBO.

Delineation of the specific types of NBO on the network formers for the dry and wet surfaces is given in Figure 15. Figure 15A shows the modifiers to which the nonbridging oxygen are attached in the dry glass surfaces, including those O that are attached to one network former and have no modifier ions within the first modifier-O first peak in the PDF (and labeled *x*SCO, where *x* is Si, Al, or B and SCO means singly-coordinated oxygen). As shown in Figure 15A, Si-NBO dominate the distribution, with most NBO interacting with Na. The NBO species labeled *x*OCaNa are formers (*x*) that have both a Ca and a Na within the first O to modifier near neighbor peak in the pair distribution function. This type of structure was previously shown in Figures 6 and 7 in our previously published simulations and discussion of these glasses.[15] Reiterating the important result previously presented regarding the presence of multiple modifiers near any particular +3 cation[15] is worthwhile here: while the simple stoichiometric concept of one +1 modifier ion charge compensating one +3 cation, or a +2 modifier charge compensating two +3 cations is correct, it misses the actual atomistic distribution of multiple modifier species around multiple +3 cations, as shown in Figures 6 and 7 from Ha and Garofalini,[15] which also means that there can be several +3 cations around any modifier ion.

Figure 15B shows the same data as 15A for the wet glass surfaces (ignoring the already presented hydroxyls), while Figure 15C shows the percent difference between the

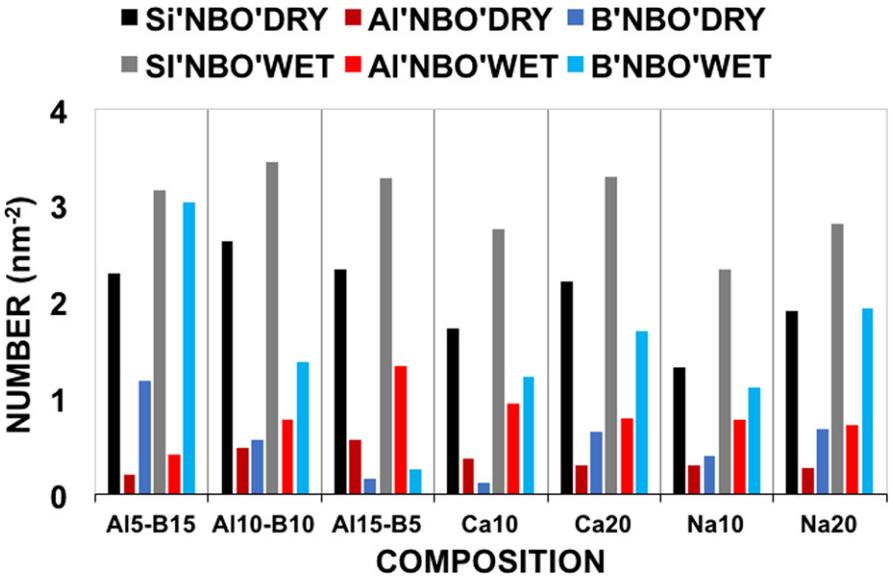

FIGURE 14 Number per nm^{-2} for all O labeled NBO that are not bridging between 2 (or 3) network formers in the dry surface versus in the wet surface. The total surface density of these NBO increase for all types in all compositions from the dry surfaces to the wet ones [Color figure can be viewed at wileyonlinelibrary.com]

dry and wet surfaces. There is a significant loss of the Si-NBO and B-NBO types in most of the glasses and less-so in the Al-NBO types. The large increase in the AlSCO is caused by the very low initial number of such species in the glass surfaces. Figure 15c indicates that the protons are predominantly displacing Na ions at NBO at the Si and B sites, with somewhat lesser displacement of the Ca at such NBO sites. Exchange of the proton for Na at NBO sites has been the classic mechanism of Na leaching from silicate glasses.

The ring size distribution was also evaluated for rings containing Si, Al, and B in the surface region of the dry glass. Figure 16A shows that, in general for all glasses, there are very few 2-membered rings, with concentrations increasing with increasing ring size except for the 6 and 8 membered rings, with the 7- and 9-membered ring distributions being similar. These larger rings can be expected due to the presence of the modifier ions that create NBO's and enable larger rings to exist. In pure SiO_2 glass, the ring sizes peak at 5-6 membered rings, with 3-membered rings in the surface in the range of ~1-2/nm^{2}.[31] The relatively large concentration of 3-membered rings is due to the

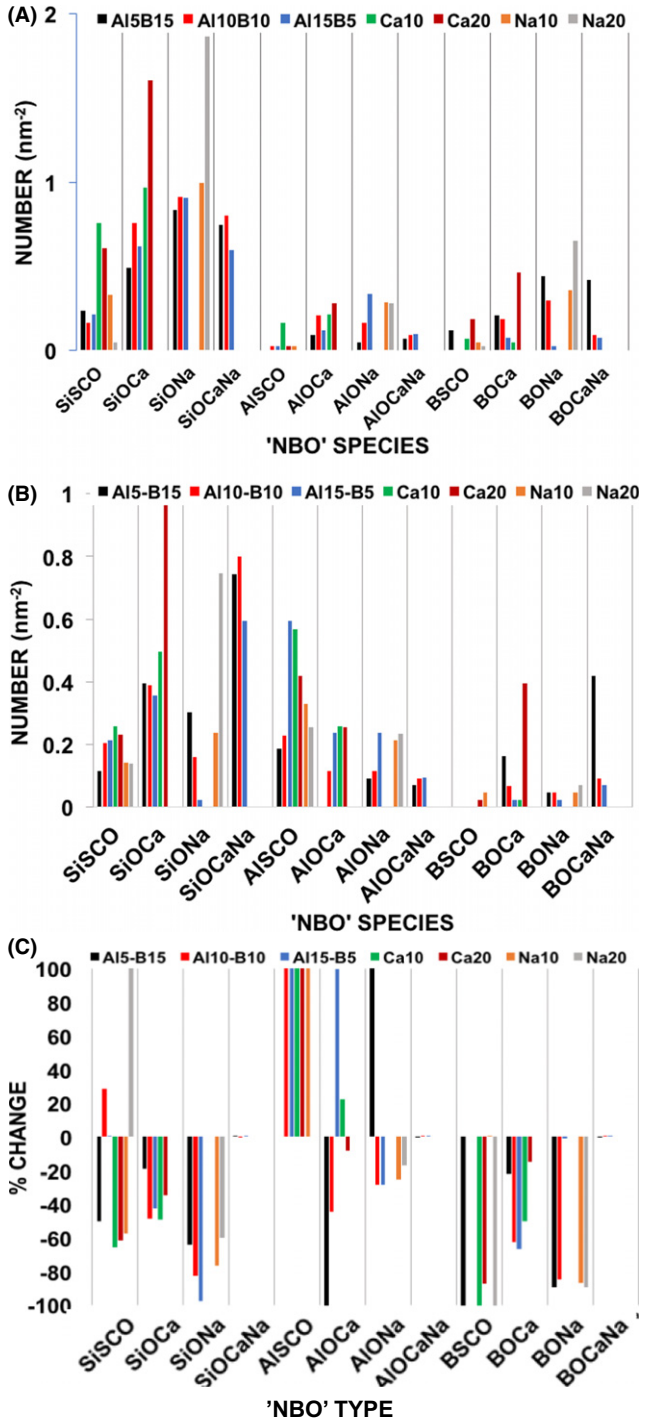

FIGURE 15 (A) Different types of NBO on the network formers in the dry glass surfaces, including singly-coordinated O (SCO) attached to only one network former and no network modifier. (B) Same as (A) except for the wet glass surfaces (hydroxyls are not included here); (C) difference in the concentrations of these surface species between the wet and dry surfaces [Color figure can be viewed at wileyonlinelibrary.com]

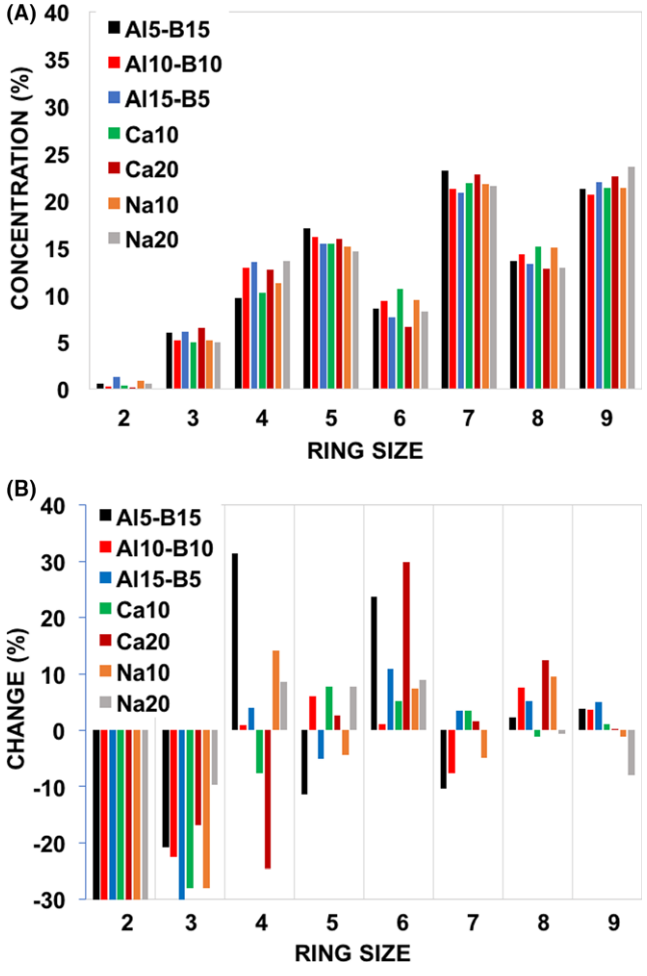

FIGURE 16 (A) Ring size distribution of rings in the surface region (surf) of the dry glasses containing Si, Al, or B cations. (B) Percent change in the ring size distribution in the glasses surface after exposure to water [Color figure can be viewed at wileyonlinelibrary.com]

presence of the Al and B, each of which has X–O–Y (X = Al or B, Y = Si, Al, or B) bond angles in the 130° range (as seen in molecular orbital calculations[44]) and thus enable stable formation of the smaller ring which has an equilibrium angle in the 130° range (as also seen in previous MD simulations of NAS glasses[22]).

Figure 16B shows the change in this distribution of ring sizes in the surface after exposure to water. The 2-membered are almost all completely removed (−100% scale not shown for elucidation of the other ring sizes). The 3-membered rings decrease the most of the remaining sizes, as expected, and the 6-membered rings in all of the glasses show an increase.

4 | CONCLUSIONS

These MD simulations involve multicomponent glasses containing Na, Ca, B, Al, Si, and O. The results indicate that a change in the angle-dependent 3-body term on the Al and B enable the simulations to more accurately reproduce the concentration of ^{4}B and ^{5}Al in the glasses without compromising the other structural features that are similar to experimental results that were previously reported. Using these more structurally accurate glasses to initially create dry surfaces in contact with a vacuum, the results show a depletion of ^{4}B at the surface in comparison to the bulk concentration for all glasses, where the surface region analyzed here is defined as the top 5-6 Å. Both subsurface (the next 10 Å below the surface) and the bulk were also analyzed. Those glasses with the lowest modifier concentrations (labeled Ca10 and Na10), in which modifier charge compensation of the +3 cations is incomplete, showed the lowest concentrations of ^{4}B in both the bulk glasses and the smallest change in the surface. This behavior is consistent with the preference of the Na for Al and Si prior to B, minimizing those available to enable formation of ^{4}B; similarly, ^{4}B is also minimized in Ca10, and Ca is not shown to specifically enhance ^{4}B formation.

Upon exposure to water, the simulations show that the ^{3}B in the top 5-6 Å of the glasses are preferentially attacked, decreasing the number of B bonds to O originally from the glass. These B become attached to only 1 or 2 O from the glass, with very little formation of B with 4 bonds to the original glass oxygen. This provides an indication of the change in the glass network. By also including B bonds to O from the water as well as the glass (i.e., all B–O bonds), there is still a decrease at the concentration of ^{3}B, but there is an increase in the concentration of ^{4}B in the surface. This increase in the concentration of ^{4}B in the surface is consistent with NEXAFS of glass surfaces containing B. The simulations show that these B are hydroxylated, forming BOH's.

There is an increase in the concentration of ^{3}Al in the dry surface in comparison to the bulk, with no ^{5}Al in the surface. However, upon exposure to water, almost all ^{3}Al are removed and converted to ^{4}Al, again with no formation of ^{5}Al.

Hydroxyl concentrations vary from 2.6-4.1 nm^{-2} for the various glasses, with SiOH and BOH dominating these surface hydroxyls (except in the high Al—low B glass, Al15-B5). Given the much lower concentration of B in the surfaces in comparison to Si, the high concentration of BOH is indicative of the initial stages of removal of the B from the glass.

Nonbridging oxygens (NBO) attached to one network former and a modifier (including a proton, or no modifier and truly singly coordinated) increase in the surface upon exposure to water, with Si-NBO and B-NBO dominating in these glasses. Delineation of the different types of NBO (xONa, xOCa, etc., where x = Si, Al, or B) show that upon exposure to water and excluding hydroxyls, the Si-NBO and B-NBO decrease the most from their dry surface concentrations. However, considering the NBO attached to a proton, forming the xOH species (x = Si, Al, B), the SiOH is ~8 times higher in concentration than any of the other Si-NBO species, the BOH are 15-20 times higher than other B-NBO species; only AlOH is in low concentration with respect to other Al-NBO. Upon exposure to water, the xNBO attached to Na are preferentially removed in the cases of x = Si or B, similar to the expected replacement of Na by the proton during leaching. In consideration of the high concentration of BOH in the wet surfaces relative to the concentration of B in the glasses and the preferential removal of xONa (x = Si or B), the simulations provide evidence of the initial stages of the eventual removal of B and Na from these glasses.

ACKNOWLEDGMENT

This research is being performed using funding received from the DOE Offices of Nuclear Energy and Environmental Management through the Nuclear Energy University Programs under Grant No. DE-NE0008597

ORCID

Stephen H. Garofalini http://orcid.org/0000-0003-1718-2034

REFERENCES

1. Kudryavtsev MY, Kolesov YI, Mikhailenko NY. Boron-free, alkali-free glass fibre for production of fibreglass-reinforced plastics. *Fibre Chem*. 2001;33:242-244.
2. Malchukova E, Boizot B. β-irradiation effect in aluminoborosilicate glasses: the role of RE codoping (RE = Sm, Gd). *Phys Sol State*. 2008;50:1687-1691.

3. Mashir YI. Optimization of the matrix compositions and properties of silver-free photochromic glasses. *Glass Ceram*. 1997;54:267-270.
4. Zhang M, Matinlinna JP. E-glass fiber reinforced composites in dental applications. *Silicon*. 2012;4:73-78.
5. Dong C, Davies IJ. Flexural properties of E glass and TR50S carbon fiber reinforced epoxy hybrid composites. *J Mater Eng Perform*. 2013;22:41-49.
6. Promis G, Bach T, Gabor A, et al. Failure behavior of E-glass fiber-and fabric-reinforced IPC composites under tension and compression loading. *Mater Struct*. 2014;47:631-645.
7. Kieu L-H, Delaye J-M, Cormier L, et al. Development of empirical potentials for sodium borosilicate glass systems. *J Non-Cryst Sol*. 2011;357:3313-3321.
8. Kieu L-H, Delaye J-M, Stolz C. Modeling the effect of composition and thermal quenching on the fracture behavior of borosilicate glass. *J Non-Cryst Sol*. 2012;358:3268-3279.
9. Bidault X, Chaussedent S, Blanc W. A simple transferable adaptive potential to study phase separation in large-scale xMg)–$(1-x)$ SiO_2 binary glasses. *J Chem Phys*. 2015;143:154501.
10. Kilinc E, Hand RJ. Mechanical properties of soda-lime-silica glasses with varying alkaline earth contents. *J Non-Cryst Sol*. 2015;429:190-197.
11. Thompson LM, Stebbins JF. Non-stoichiometric non-bridging oxygens and five-coordinated aluminum in alkaline earth aluminosilicate glasses: effect of modifier cation size. *J. Non Cryst. Sol*. 2012;358:1783-1789.
12. Wu J, Stebbins JF. Temperature and modifier cation field strength effects on aluminoborosilicate glass network structure. *J Non-Cryst Sol*. 2013;362:73-81.
13. Wu J, Stebbins JF. Quench rate and temperature effects on boron coordination in aluminoborosilicate melts. *J Non-Cryst Sol*. 2010;356:2097-2108.
14. Wu J, Stebbins JF. Effects of cation field strength on the structure of aluminoborosilicate glasses: high-resolution 11B, 27Al, and 23Na MAS NMR. *J Non-Cryst Sol*. 2009;355:556-562.
15. Ha M-T, Garofalini SH. Local structure of network modifier to network former ions in soda-lime-alumino-borosilicate glasses. *J Am Ceram Soc*. 2017;100:563-573. https://doi.org/10.1111/jace.14565.
16. El-Damrawi G, Muller-Warmuth W, Doweidar H, et al. 11B, 29Si, and 27Al nuclear magnetic resonance studies of Na_2O–Al_2O_3–$B2O_3$–SiO_2 glasses. *Phys Chem Glasses*. 1993;34:52-57.
17. Lee SK, Stebbins JF. The structure of aluminosilicate glasses: high-resolution 17O and 27Al MAS and 3QMAS NMR study. *J Phys Chem B*. 2000;104:4091-4100.
18. Du L-S, Stebbins JF. Network connectivity in aluminoborosilicate glasses: a high-resolution 11 B, 27 Al and 17 O NMR study. *J Non-Cryst Sol*. 2005;351:3508-3520.
19. Melman H, Garofalini SH. Microstructural evaluation of simulated sodium silicate glasses. *J Non-Cryst Solids*. 1991;134:107-115.
20. Newell RG, Feuston BP, Garofalini SH. The structure of sodium trisilicate glass via molecular dynamics employing three-body potentials. *J Mater Res*. 1989;4:434-439.
21. Zirl DM, Garofalini SH. Structure of sodium-aluminosilicate glass surfaces. *J Am Ceram Soc*. 1992;75:2353-2362.
22. Zirl DM, Garofalini SH. Structure of sodium-aluminosilicate glasses. *J Am Ceram Soc*. 1990;73:2848-2856.
23. Su X, Garofalini SH. Atomistic structure of calcium silicate intergranular films between prism and basal planes in silicon nitride: a molecular dynamics study. *J. Mat. Res*. 2004;19:752-758.
24. Blonski S, Garofalini SH. Atomistic structure of calcium silicate intergranular films in alumina studied by molecular dynamics simulations. *J Am Ceram Soc*. 1997;80:1997-2004.
25. Garofalini SH, Luo W. Molecular dynamics simulations of calcium silicate intergranular films between silicon nitride crystals. *J Am Ceram Soc*. 2003;86:1741-1752.
26. Garofalini SH. Molecular Dynamics Simulations of Glass Surfaces and Interfaces. In: Cygan R, Kubicki J, eds. *Reviews in Mineralogy and Geochemistry: Molecular Modeling Theory: Applications to the Geosciences*. Vol. 42. Washington DC: Mineralogical Society of America; 2001:131-164.
27. Adelstein N, Olsen CS, Lordi V. Hole traps in sodium silicate: first-principles calculations of the mobility edge. *J Non-Cryst Sol*. 2015;430:9-15.
28. Pinto HP, Nieminen RM, Elliott SD. Ab initio study of the gamma-Al_2O_3 surfaces. *Phys Rev B.*. 2004;70:125402/1-11125402.
29. Garofalini SH. A molecular dynamics simulation of the vitreous silica surface. *J Chem Phys*. 1983;78:2069-2072.
30. Feuston BP, Garofalini SH. Water-induced relaxation of the vitreous silica surface. *J Appl Phys*. 1990;68:4830-4836.
31. Feuston BF, Garofalini SH. Topological and bonding defects in vitreous silica surfaces. *J Chem Phys*. 1989;91:564-569.
32. Garofalini SH. Molecular dynamics computer simulations of silica surface structure and adsorption of water molecules. *J Non-Cryst Solids*. 1990;120:1-12.
33. Mahadevan TS, Garofalini SH. Dissociative chemisorption of water onto silica surfaces and formation of hydronium ions. *J Phys Chem C*. 2008;112:1507-1515.
34. Benoit M, Profeta M, Mauri F, et al. First-principles calculation of the 17O NMR parameters of a calcium aluminosilicate glass. *J Phys Chem B*. 2005;109:6052-6060.
35. Brown G, Waychunas G, Ponader C, et al. EXAFS and NEXAFS studies of cation environments in oxide glasses. *J de Phys*. 1986;47:140-147.
36. Schmücker M, Schneider H, MacKenzie K, et al. Comparative 27 Al NMR and LAXS studies on rapidly quenched aluminosilicate glasses. *J Eur Ceram Soc*. 1999;19:99-103.
37. Emme H, Huppertz H. High-pressure preparation, crystal structure, and properties of α-(RE) 2B4O9 (RE = Eu, Gd, Tb, Dy): oxoborates displaying a new type of structure with edge-sharing BO_4 tetrahedra. *Chem-A Eur J*. 2003;9:3623-3633.
38. Doweidar H, Moustafa Y, El-Maksoud SA, et al. Properties of Na_2O–Al_2O_3–B_2O_3 glasses. *Mater Sci Eng: A*. 2001;301:207-212.
39. Toplis MJ, Dingwell DB. Shear viscosities of CaO–Al_2O_3–SiO_2 and MgO–Al_2O_3–SiO_2 liquids: implications for the structural role of aluminum and the degree of polymerisation of synthetic and natural aluminosilicate melts. *Geochim Cosmochim Acta*. 2004;68:5169-5188.
40. Allwardt JR, Lee SK, Stebbins JF. Bonding preerences of non-bridging O atoms: evidence from 17O MAS and 3QMAS NMR on calcium aluminate and low-silica Ca-aluminosilicate glasses. *Am Mineral*. 2003;88:949-954.
41. Kelso J, Pantano CG, Garofalini SH. A comparison of ions scattering spectra and molecular dynamics simulations at the surface of silicate glass. *Surf Sci*. 1983;134:L543-L549.

42. Garofalini SH, Levine S. Differences in surface behavior of alkali ions in Li_2O $3SiO_2$ and Na_2O $3SiO_2$ glasses. *J Am Ceram Soc*. 1985;68:376-379.
43. Schaut RA, Lobello RA, Mueller KT, et al. Characterization of boroaluminosilicate glass surface structures by B K-edge NEXAFS. *J Non-Cryst Sol*. 2011;357:3416-3423.
44. Geisinger KL, Gibbs GV, Navrotsky A. A molecular orbital study of bond length and angle variations in frameowork structures. *Phys Chem Miner*. 1985;11:266-283.

SUPPORTING INFORMATION

Additional Supporting Information may be found online in the supporting information tab for this article.

How to cite this article: Garofalini SH, Ha MT, Urraca J. Simulations of the surfaces of soda lime aluminoborosilicate glasses exposed to water. *J Am Ceram Soc*. 2018;101:1135–1148. https://doi.org/10.1111/jace.15237